Dynamics of tracheal compression in the horned passalus beetle

James S. Waters, Wah-Keat Lee, Mark W. Westneat and John J. Socha

Am J Physiol Regul Integr Comp Physiol 304:R621-R627, 2013. First published 20 February 2013; doi: 10.1152/ajpregu.00500.2012

Am J Physiol Regul Integr Comp Physiol 304: R621–R627, 2013.
First published February 20, 2013; doi:10.1152/ajpregu.00500.2012.

Dynamics of tracheal compression in the horned passalus beetle

James S. Waters,[1] Wah-Keat Lee,[2] Mark W. Westneat,[3] and John J. Socha[4]

[1]*Department of Ecology and Evolutionary Biology, Princeton University, Princeton, New Jersey;* [2]*Advanced Photon Source, Argonne National Laboratory, Argonne, Illinois;* [3]*Department of Zoology, Field Museum of Natural History, Chicago, Illinois; and* [4]*Department of Engineering Science and Mechanics, Virginia Tech, Blacksburg, Virginia*

Submitted 1 November 2012; accepted in final form 16 February 2013

Waters JS, Lee W, Westneat MW, Socha JJ. Dynamics of tracheal compression in the horned passalus beetle. *Am J Physiol Regul Integr Comp Physiol* 304: R621–R627, 2013. First published February 20, 2013; doi:10.1152/ajpregu.00500.2012.—Rhythmic patterns of compression and reinflation of the thin-walled hollow tubes of the insect tracheal system have been observed in a number of insects. These movements may be important for facilitating the transport and exchange of respiratory gases, but observing and characterizing the dynamics of internal physiological systems within live insects can be challenging due to their size and exoskeleton. Using synchrotron X-ray phase-contrast imaging, we observed dynamical behavior in the tracheal system of the beetle, *Odontotaenius disjunctus*. Similar to observations of tracheal compression in other insects, specific regions of tracheae in the thorax of *O. disjunctus* exhibit rhythmic collapse and reinflation. During tracheal compression, the opposing sides of a tracheal tube converge, causing the effective diameter of the tube to decrease. However, a unique characteristic of tracheal compression in this species is that certain tracheae collapse and reinflate with a wavelike motion. In the dorsal cephalic tracheae, compression begins anteriorly and continues until the tube is uniformly flattened; reinflation takes place in the reverse direction, starting with the posterior end of the tube and continuing until the tube is fully reinflated. We report the detailed kinematics of this pattern as well as additional observations that show tracheal compression coordinated with spiracle opening and closing. These findings suggest that tracheal compression may function to drive flow within the body, facilitating internal mixing of respiratory gases and ventilation of distal regions of the tracheal system.

bessbug; biomechanics; convection; insect; tracheae

INSECT RESPIRATION IS A COMPLEX biomechanical, physiological, and behavioral system. Physically, gas transport through insect tracheae involves a combination of diffusive and convective mechanics (3, 24, 30, 40). Physiologically, the control and regulation of respiratory patterns are subject to developmental and environmental conditions (2, 11–13, 22, 26–28). Body posture and movement may influence the demand for gas exchange and also affect the regulation and transport of respiratory gases (1, 33).

Historically, one of the primary tools for investigating the complexity of insect respiration has been the study of external gas exchange (24), with a focus on patterns of carbon dioxide emission enabled by the ease and accuracy of CO_2 measurements using modern techniques (2, 5, 9, 23, 25). Such studies have provided extensive knowledge and insight into the respiratory physiology of insects (8, 21, 29), but we know almost nothing about what happens to the air between the spiracle entrance to the tracheal system and the terminal branches of the tracheae embedded within the insect's tissues. The specific mechanics of insect respiratory systems largely remain a "black box" due to the difficulty of measuring and sensing the microenvironment within live insects. Although diffusion-only systems can be modeled with a static geometry, patterns of exchange in insects that create bulk flow of air by changes in tracheal system volume require the understanding of patterns of compression or expansion in the tracheal system.

The applicability of synchrotron X-ray phase-contrast imaging for studying small animals has made it possible to observe the internal structure and dynamics of insect tracheal systems in vivo (36, 42). Contrary to the long-standing paradigm that insect tracheae function largely as rigid conduits, many tracheae and air sacs exhibit periodic deformations. The rhythmic collapse and reinflation of localized regions of the tracheal system have been observed in a range of adult insects, including ants (41), beetles (35, 41), flies (34), crickets, and grasshoppers (14, 18, 41). Recent work has shown that even soft-bodied animals can exhibit tracheae that compress; late-instar *Manduca sexta* caterpillars switch to rhythmic compression (from none) under hypoxic conditions (15). The documented records of tracheal tube deformation have suggested that compression is synchronous between tubes and may be spatially symmetrical within a tube (35, 41). However, few details on the kinematics of tube collapse have been reported. Given that multiple physical mechanisms may underlie the generation of tube collapse, it is possible that insects exhibit substantial variation in collapse kinematics. Here, we report observations of new patterns of tracheal compression in the horned passalus beetle, *Odontotaenius disjunctus* Illiger (Coleoptera: Passalidae).

Odontotaenius disjunctus is a social, primarily flightless beetle that excavates tunnels and galleries within rotting hardwood, with a distribution that is widespread across the United States and extends south into the tropics (10). It is relatively large for an insect, with a body mass on the order of 1 g, and with correspondingly large tracheal structures. A single prior study has examined the respiratory anatomy of this species (32). The major structures of the tracheal system include tubular tracheae, so-called "collapsible tracheae," and air sacs (32). Robertson observed that both tubular and collapsible tracheae contained reinforcing chitinous spiral-strand taenidiae, but the air sacs did not. Regionally, air sacs are found only in the head and thorax, and collapsible tracheae are confined to the abdomen. Robertson hypothesized that, because air sac tissue lacks reinforcing taenidia, the air sacs may function as a bellows to inflate the major tracheal trunks, and, additionally, that the collapsible tracheae might serve a similar function in the abdomen. His anecdotal support for this hypothesis was found in observations of rhythmic bellows-like movement of the thin-walled dorsolateral metathoracic cuticle, which could produce the hypothesized tracheal movements. However, Robertson (32) was unable to directly observe the tracheal system in the living beetle,

Address for reprint requests and other correspondence: James S. Waters, Dept. of Ecology and Evolutionary Biology, Princeton Univ., Princeton, NJ 08544, USA (e-mail: jswaters@princeton.edu).

and all of his functional conclusions were based on inferences from anatomical dissections. Here, we use X-ray imaging to visualize movements of the air-filled tracheae within live, intact, passalid beetles. Specifically, we identify tracheal tubes that exhibit substantial deformations and describe their detailed dynamics for the first time.

METHODS

We recorded live video of the tracheal system of adult horned passalus beetles (*Odontotaenius disjunctus*) using synchrotron X-ray phase-contrast imaging. All experiments were conducted at the Advanced Photon Source (APS) at Argonne National Laboratory (Argonne, IL). Beetles were purchased from Carolina Biological Supply (Burlington, NC) and shipped directly to the APS. The average wet mass of live beetles was 1.57 ± 0.07 g, and the average body length was 34.1 ± 1.7 mm (mean ± SD). Live beetles were placed within a tube of X-ray transparent polyimide film (Kapton, Dupont, DE) and were positioned horizontally above a set of mechanical translation and rotation stages. Although this enclosure held the beetle in place, it was loose enough to allow the beetle to move its head, legs, and abdomen within the tube, and included holes for access to ambient air. We used monochromatic X-rays with an energy of 25 keV and a sample-to-detector distance of 0.8 m; other beam settings and experimental protocols were consistent with those of previous studies (35, 36). X-ray videos from a Cohu 4920 video camera (Cohu, San Diego, CA) were recorded at standard video rates (30 Hz) onto MiniDV tapes with an image size of 720 × 480 pixels and a field of view of 3.3 by 2.5 mm.

We focused the imaging field of view on the major longitudinal tracheal tubes in the thorax. A total of 4 h of X-ray video were recorded across five animals (average, 44 min per specimen). During much of the recorded video, the beetle's movement made it difficult to observe the tracheae, but during stationary periods, it was possible to repeatedly observe specific tracheal tubes. Additionally, in one specimen, these tracheae and a mesothoracic spiracle could be identified within the same field of view. We digitized video recordings of tracheal dynamics and used QuickImage software (38) to quantify patterns of tracheal compression.

To precisely quantify the kinematics of compression in the major tracheae, we focused on the pair of superior cephalic tracheae, which occurred in the most prominent region of tracheal compression. This pair of tracheal tubes originates from the tracheal atrium connected to the mesothoracic spiracle and extends through the thorax and into the head (Fig. 1, *A* and *B*). We quantified the tracheal diameter as a function of both time and position along the longitudinal axis of the tube by measuring the width of the trachea at three sequential positions, all simultaneously visible for the duration of the compression cycle (Fig. 2*A*). The three widths were measured ~300 μm apart, covering an average trachea length of 1.0 mm. Tracheal position coordinate data were digitized for each frame of video for eight complete compression cycles, averaging ~183 frames (6.1 s) per compression cycle.

The digitized kinematic data were used to characterize the dynamics of compression in the superior cephalic tracheae. We determined the rates of tube collapse and reinflation and the sequence of these changes along the length of the tracheal tube. We also calculated the average periods during which the tracheal tube was fully inflated (the "resting" state) and collapsed (the "compressed" state). To calculate the speed of propagation of compression and reinflation in the axial direction, we calculated the distance between sequential pairs of points and determined how much time was necessary for the compression (and reinflation) to reach its peak rate of change (i.e., maximum derivative) at each of the three sequential positions along the length of the tube. For the animal in which we were able to observe the mesothoracic spiracle concurrently with the tracheal trunks, we recorded the time codes associated with the spiracle's opening and closing and tracheal compression cycles to determine the temporal relationship between these behaviors. Means are reported

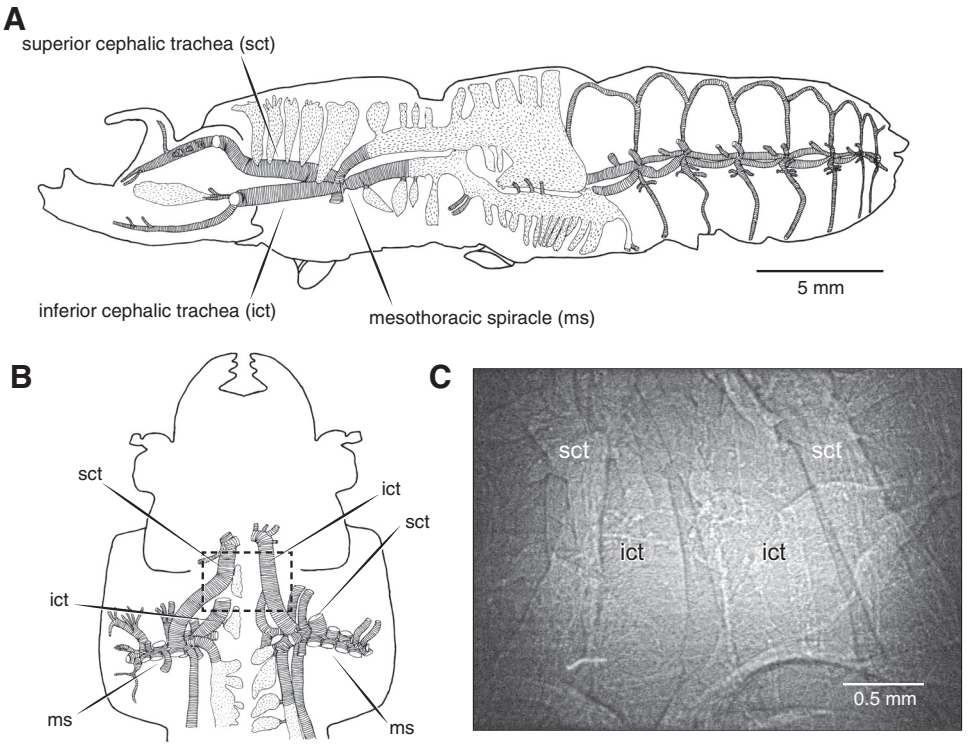

Fig. 1. The general anatomy of the tracheal system of *Odontotaenius disjunctus*. The schematics (*A* and *B*) show the system from lateral and dorsoventral perspectives, respectively, as modified from Robertson (32). *C*: superior cephalic tracheae (sct) and inferior cephalic tracheae (ict) as visualized within a live *O. disjunctus* using synchrotron X-ray phase-contrast imaging. The beetle is oriented as in *B*, with the dorsoventral plane perpendicular to the X-ray beam; the field of view is shown by the dotted-line box in *B*.

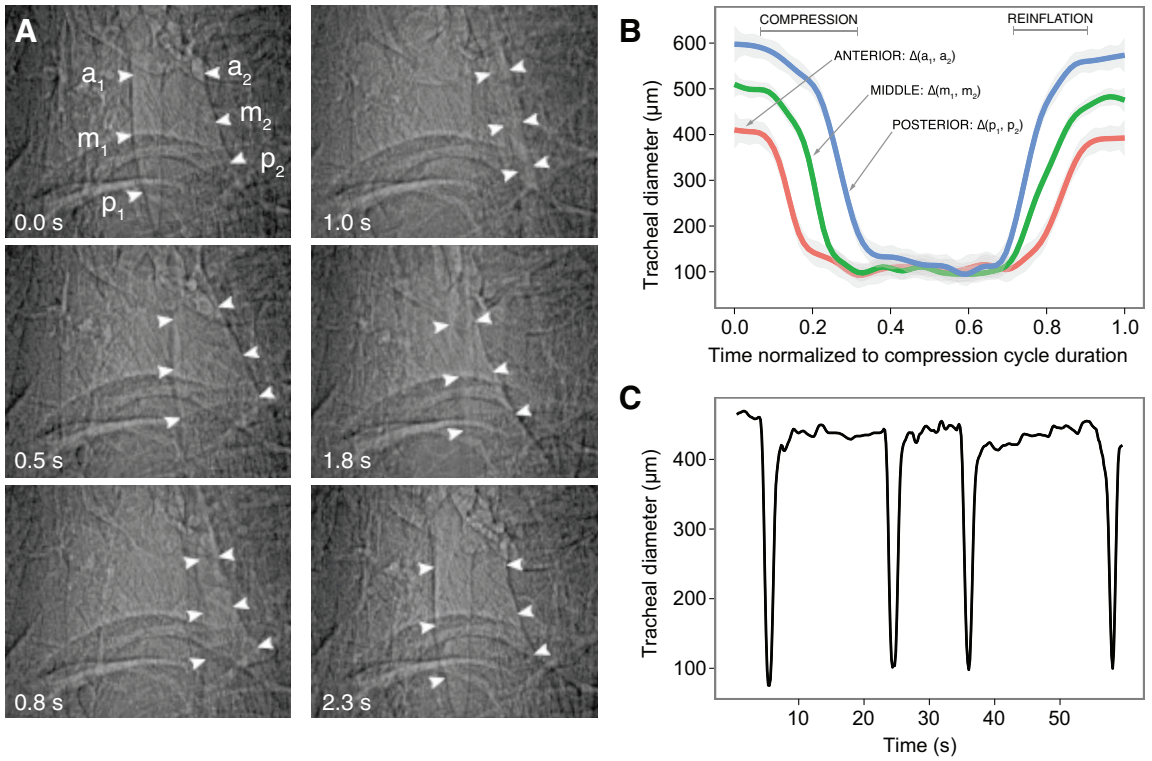

Fig. 2. Bidirectional tracheal compression in *O. disjunctus*. *A*: these six video frames (cropped for clarity) show the sequence of tracheal compression in the right superior cephalic trachea. The beetle is positioned as in Fig 1, *B* and *C*; the head is at the top, and the mesothorax is at the bottom of each frame. The axial propagation of compression takes place from 0.0 to 1.0 s; the tube remains compressed from 1.0 to 1.8 s and reinflates in reverse from 1.8 to 2.3 s. Arrowheads indicate positions along the visualized edge of the trachea that were digitally tracked to estimate changes in tracheal diameter as a function of time. *B*: kinematics of tracheal compression in the prothoracic tracheae reveal a sequential, wave-like compression propagating along the longitudinal axis of the trachea. This figure plots the changes in tracheal diameter as a function of time and also according to axial position, as indicated by the three lines that correspond to the three pairs of arrowheads in *A*. The order of reinflation back along the longitudinal axis of the trachea is the reverse of its order for compression. *C*: tracheal compression and reinflation cycles plotted here are based on digitizing tracheal diameter using a single pair of coordinates and indicate the behavior of this system over a 60-s time window. The duration of the compression and reinflation cycle is less than the period between compressions, during which the trachea remains relatively stationary and inflated.

throughout with SE, and statistical analyses were carried out using Prism 5.0 (GraphPad Software, San Diego, CA) and R 2.13 (31).

RESULTS

The superior cephalic tracheae (Fig. 1*C*) in the head and thorax of *O. disjunctus* exhibited a wavelike pattern of compression and reinflation (Fig. 2; Supplemental Movie S1). These events occurred periodically with 8.52 ± 0.58 s between the initiation of sequential compression cycles. When fully compressed, the tracheal widths decreased by 77 ± 4%. The tracheal walls along the length of the compressing region did not collapse at the same time, but rather in a continuous sequential pattern (Fig. 2). The compression initiated in the cephalic region, where the back of the head capsule is withdrawn into the anterior prothorax and propagated down the longitudinal axis of the trachea into the posterior prothorax with an average velocity of 4.4 ± 1.4 mm/s. After compressing, the tubes remained collapsed for 0.98 ± 0.10 s. Reinflation proceeded in the reverse order, beginning where the compression ended in the posterior prothorax and expanding with an average velocity of −9.6 ± 1.3 mm/s toward the anterior prothorax and head capsule. The axial propagation speed of compression was significantly slower than the rate of expansion (paired *t*-test, $t = -2.7$, df = 7, $P = 0.029$). The average period between compression cycles during which the tracheae remained inflated was 5.92 ± 0.57 s.

Although it was not possible to view the entire prothorax and head in the same frame, it was possible to observe simultaneous compressions of the left and right superior cephalic tracheae (Supplemental Movie S2). The spatial extent of compression in these tracheae covered at least 1.24 ± 0.13 mm in tracheal length, extending from the posterior head to approximately midway through the prothorax and terminating above the first leg coxae. In contrast, the inferior cephalic tracheae did not appear to exhibit tracheal compression cycles.

Compressions were observed to occur in other tracheae in the head, thorax, and abdomen. In the head, compressions were observed in small tracheae in the mandibles and horn. In the thorax, tracheae extending from the atria of the mesothoracic and metathoracic spiracles exhibited compressions with roughly the same frequency as the dorsal cephalic tracheae. Also, sac-like tracheae that surround the abdomen around the lateral margins exhibited periodic compression with dynamics similar to the other observed tracheal compressions.

For one beetle, we were able to directly observe the opening and closing of the left mesothoracic spiracle in combination with tracheal compression and reinflation cycles (Fig. 3, Supplemental Movie S3). In a period of 104 s, the mesothoracic

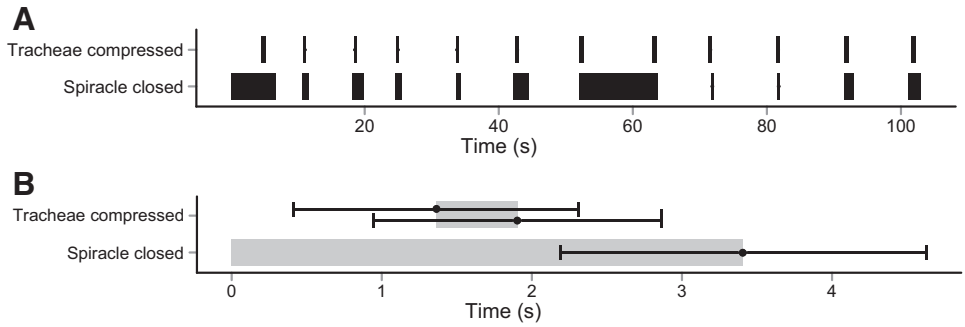

Fig. 3. The relationship between tracheal tube collapse and mesothoracic spiracle movement in the thorax. *A*: timing of spiracle opening and closing correlates with the timing of tracheal compression. *B*: this plot summarizes the overlapping timing of spiracle closure and tracheal compression for 12 sequential cycles of tracheal compression. The timing for each cycle was referenced on the basis of the start of the spiracle's closure. The solid gray bars indicate the average duration of spiracle closure and duration of tracheal compression. Error bars indicate the standard error of the duration of spiracle closure and the standard error among the distribution of start and stop times of tracheal compression relative to the spiracle's closure. See Fig. 1, *A* and *B* for position of the mesothoracic spiracle with respect to the thoracic tracheae and Supplemental Movie S3 on the journal's website for a video recording of these observations.

spiracle (ms, Fig. 1, *A* and *B*) opened and closed 11 times. During the same period, the tracheal tubes extending from the spiracular atrium exhibited 12 cycles of compression and reinflation. The timing of spiracle closing was highly correlated with the timing of tracheal compression ($r = 0.49$, $P < 0.001$). In particular, tracheal compression occurred when the spiracle was closed (11 of 12 events); in one event, compression occurred just prior to closing. The state of the other spiracles during these observations is not known.

DISCUSSION

Insects have evolved tracheal systems that enable them to be extraordinarily successful taxa across a wide range of environmental conditions and to exhibit impressive flexibility in behavioral phenotypes (4). As a relatively large, fungus-cultivating beetle that excavates galleries within decaying hardwood logs, the horned passalus beetle may engage in its most metabolically demanding behaviors within the ecophysical constraints of environmental hypoxia (17, 20). Observing the real-time behavior of insect tracheae is the first step toward understanding the physiological mechanisms that generate dynamic patterns of air flow within the tracheal system. These mechanisms and the patterns of airflow that they generate may have been critical factors influencing the evolution of this species' body size and ecological niche (10, 19).

We examined the compression kinematics of tracheae in the horned passalus beetle and found a unique compression pattern in which collapse occurred sequentially in one direction along the tube length and then reinflation occurred in the opposite direction. The sequential and reversed directionality within a complete compression cycle indicates that these compressions produced two distinct forms of air movement. If so, this system represents a respiratory structure that functions as a pump that transports air bidirectionally within the insect's tracheal system.

Although it is apparent that tracheal compressions displace tracheal air and, therefore, must produce bulk flow, it is relevant to consider whether convection or diffusion is the dominant mechanism of transport in the large tracheae. To address this question, we developed two analytical models to estimate the dynamics of diffusive and convective airflow within a tracheal tube (see APPENDIX). We considered a hollow cylinder (5 mm in length; 0.5 mm in diameter) similar to the dorsal cephalic tracheae. Given a set of spatial and temporal boundary conditions chosen to generate the maximal diffusive capacity, the diffusion model predicts that the flux of oxygen at the distal end of the tracheal tube reaches a maximum of 0.0036 μmol/s at 0.57 s and decreases to 0.0014 μmol/s after 10 s (Fig. 4). These rates correspond to 2.02–5.19 μl O_2/min at 20°C. Similarly, during the collapse phase of a compression-reinflation cycle, the convection model predicted a peak oxygen flux of 0.0015 μmol/s (2.17 μL O_2/min). While both mechanisms appear capable of generating comparable flux rates, considered over the duration between sequential tracheal compression cycles, the average convective flux across the complete compression and reinflation cycle is only 0.0002 μmol/s (0.29 μl O_2/min), an order of magnitude less than the estimates for diffusive transport. However, and perhaps more importantly, because compression and inflation waves travel in opposite directions, it is possible that this mechanism moves air in both directions, resulting in little or no net flow, and also potentially driving flow against the diffusion gradients for either oxygen or carbon dioxide.

By this analysis, our model suggests that compression in the horned passalus beetle augments transport of gases relative to that attainable by diffusion alone. Of particular interest is how rates of diffusive and convective flows change over time and how these transport processes may correlate with the timing of spiracle opening. Our model predicts that the rate of diffusive flux decreases from its maximum to the rate attainable by convective transport during tracheal compression over ~8 s, a duration of the same order of magnitude as the period between tracheal compression cycles.

Determining the importance of convection and diffusion can also be approached more generally by calculating the Péclet number (37). The Péclet number is a dimensionless number that compares transport of a substance by bulk flow vs. transport by diffusion using the following equation: $Pe = (vl/D)$, where v is velocity of the moving fluid, l is the length scale of transport, and D is the diffusion coefficient. Here, we assume that the velocity of the air is equal to the translational velocity of the compression along the length of the tube. Using a tube length of 5 mm, velocities of 4.4 mm/s (compression) and 9.6 mm/s (reinflation), and a diffusion coefficient of 0.219 cm^2/s,

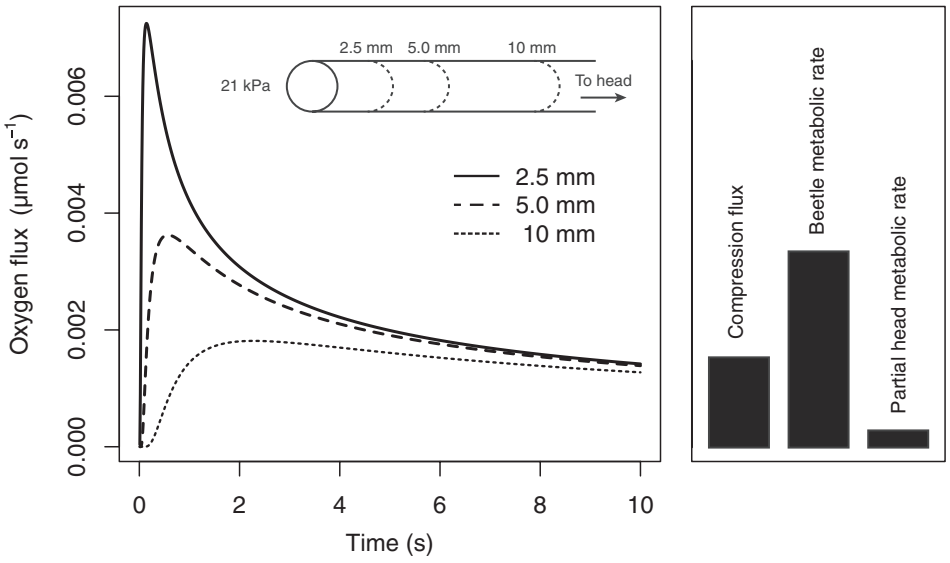

Fig. 4. The temporal dynamics of oxygen diffusion at three different lengths along a tracheal tube, modeled using the differential form of Fick's first law. Using the same ordinate scale, the bar graph on the right side illustrates an estimate for the peak convective flow during compression, a reported measurement for the metabolic rate (1611.6 μW) of a 1.63 g *O. disjunctus* (6), and an estimate of the fraction of whole animal metabolic rate supplied by the single tracheal tube.

the Péclet number ranges from 1.0 to 2.2. This suggests that neither diffusion nor convection dominates the transport during tracheal compression, a conclusion that is congruent with the analytical modeling analysis.

This study also reports for the first time the exact coordination of tracheal movements with spiracle opening and closing. The synchronization of spiracle opening and closing with tracheal compression could have a dramatic influence on the pressure gradients and patterns of air flow during tracheal compression cycles. For instance, consider a spiracle and its locally connected tracheal tubes. If the tracheae compress when the spiracle is open, a large fraction of the displaced gas is likely to be transported toward the spiracle and out of the body, assuming that the resistance to flow is much lower in the outward direction. Conversely, if the spiracle is closed, the air must be transported away from the spiracle and deeper into the body. We observed 12 cycles of tracheal compression that coincided with the mesothoracic spiracle closure (Fig. 3). In every compression event, the spiracle was closed or in the process of closing. The correlation between spiracle closure and tracheal compression suggests a novel hypothesis for the role of tracheal compression, which is to transport air toward more distal regions of the body, possibly including the head, legs, and antennae. This transport of air within body regions may also increase the mixing of gases within the tracheal system. Intriguingly, our results are consistent with the predictions of a model for the water economy of insects, in which simultaneous spiracle closure and tracheal compression are proposed as a mechanism to condense water vapor within the tracheal system to either redistribute water between body regions or minimize evaporative water loss (7). To test this model, future studies may manipulate relative humidity around an insect within a chamber and observe whether or not water vapor pressure has a causal effect on dynamics of tracheal compression or the synchrony of tracheal compression and spiracle closure.

The observation that tracheal compression is slower than reinflation is consistent with the idea that elastic energy is stored in the tracheal wall during compression, and reinflation occurs as a passive process of energy return, with dynamics governed by the viscoelastic properties of the trachea (39). Variation in structural properties of the tracheae, including thickness, second-moment of area, and taenidia geometry, might play functional roles in storing and releasing energy during cycles of compression and reinflation. Alternatively, the compression may be slower than expansion, if, while the spiracle is closed, more force is required to push air into the distal regions of the tracheal system (e.g., into peripheral air sacs, the head, or extremities) against the pressure generated by holding the local spiracles sealed. Lastly, it is possible that the differences in kinematics can be explained by differences in the rates of hemolymph pressure changes if this mechanism controls the tracheal deformation.

Perspectives and Significance

Investigating the behavior and dynamics of insect tracheal system structures is necessary to develop an integrative understanding of respiratory physiology at the organismal level. Here, we describe the kinematics of tracheal compression in the two dorsal cephalic trunks, but further work is needed to understand this complex system, in particular, with respect to the tracheal ultrastructure and with respect to the elaborate system of branching tracheae and air sacs. We focused on one region of the tracheal system of this large beetle, but sequential and asymmetric tracheal compressions may occur in other body regions, influencing patterns of air sac inflation and potentially coordinated with spiracular control. These compression patterns may enhance this species' hypoxia tolerance and its performance of energetically demanding behaviors, including excavation and stridulation. Additionally, if tracheal compression cycles increase the efficiency of mixing within the tracheal system, it may allow the animal to close its spiracles for an extended duration, with potential beneficial consequences for desiccation resistance and mite protection (7, 10, 16). This study suggests that air movement patterns within the respiratory systems of insects are more complex than is currently appreciated and that further determination of compression patterns across insects is worthy of detailed investigation.

APPENDIX

Convection model. The peak bulk flow of oxygen produced by tracheal compression can be modeled on the basis of estimating the change in tracheal volume. We assumed that the tracheal lumen contains air with an ambient oxygen concentration (u_0, mol of O_2 cm^{-3}) and that the tube has a cylindrical geometry characterized by a constant length (l, cm) and a radius (r, cm) that varies with the extent of tracheal compression. Finally, given a compression period (t, s), during which the tracheal tube collapses (i.e., not including the time for reinflation) and assuming that the displaced air flows in a single direction during this collapse, the flux (Q, mol of O_2 per second) may be calculated by

$$Q_{\text{convection}} = u_0 \frac{\pi l}{t}(r_{\max}^2 - r_{\min}^2)$$

Diffusion model. Fick's first law is an equation that predicts diffusive flux (J, mol of O_2/s per cross-sectional area) as a function of a diffusion coefficient (D, cm^2/s) and a spatial concentration gradient ($\partial u/\partial x$). In one dimension, with respect to distance (x) and time (t), Fick's first law is

$$J = -D\frac{\partial}{\partial x}u(x, t)$$

Modeling the temporal dynamics of the changing spatial concentration gradient requires a solution to Fick's second law, which describes the relationship between the concentration gradients in time and space:

$$\frac{\partial}{\partial t}u(x, t) = D\frac{\partial^2 u}{\partial x^2}$$

The solution to this equation is a function, $u(x,t)$, which gives the concentration of the diffusing substance as a function of distance and time, depending on particular boundary and initial conditions. In our case, oxygen concentration at one boundary may be fixed at a constant value (e.g., the atmospheric oxygen concentration, u_0), and it may not be predefined at the distal boundary condition. Since a second boundary condition is necessary for a solution, we can also define the rate of change of oxygen at the source boundary as zero. For this situation, we can, thus, define two boundary conditions and one initial condition for $0 \le x \le \infty$ and $0 \le t$:

$$u(0, t) = u_0$$

$$\frac{\partial}{\partial t}u(0, t) = 0$$

$$u(x, 0) = 0$$

Given these conditions, the solution to the diffusion equation in one dimension is

$$u(x, t) = u(0, t)\frac{2}{\sqrt{\pi}}\int_{\frac{x}{2\sqrt{Dt}}}^{\infty} e^{-t^2}dt$$

Taking the derivative of this solution with respect to distance gives

$$\frac{\partial}{\partial x}u(x, t) = u(0, t)\frac{-1}{\sqrt{\pi Dt}}e^{\frac{-x^2}{4Dt}}$$

Substituting this expression back into Fick's first law gives an expression for the temporal dynamics of diffusive flux (Q, mol/s) at a distance (L, cm) within a cylindrical tube with a constant radius (r, cm):

$$Q_{\text{diffusion}} = u_0 r^2 \sqrt{\frac{\pi D}{t}} e^{\frac{-L^2}{4Dt}}$$

These equations make it possible to model the spatial and temporal dynamics of air flow within a tracheal tube, but the predictions must be evaluated in the context of the general assumptions and explicit boundary conditions. It is unlikely, for example, that the oxygen partial pressure gradient within a single tracheal tube is ever as high as in the diffusion model. Future explorations of this model may incorporate the effects of a radial concentration gradient (across the tracheal wall), as well as experimentally parameterized boundary conditions.

ACKNOWLEDGMENTS

We thank Kamel Fezzaa for technical assistance, and Jon Harrison, Jaco Klok, Hodjat Pendar, Jennifer Fewell, and Michael LaBarbera for valuable feedback on previous drafts of the manuscript. Rebecca Zapata adapted Robertson's 1962 anatomical illustration in Fig. 1. We also acknowledge many helpful discussions with colleagues in the Harrison Laboratory at Arizona State University, the Socha Laboratory at Virginia Tech, and with students of Michael LaBarbera's Biomechanics of Organisms course at The University of Chicago. We are grateful for the insightful feedback offered by four reviewers. Use of the Advanced Photon Source, an Office of Science User Facility operated for the U.S. Department of Energy (DOE) Office of Science by Argonne National Laboratory, was provided by the U.S. DOE under contract no. DE-AC02-06CH11357.

GRANTS

The Charlotte Mangum Student Support Program made it possible for J. S. Waters to present these findings at the annual meeting of the Society for Integrative and Comparative Biology. J. J. Socha was supported by the National Science Foundation under Grant 0938047 and by the Virginia Tech Institute for Critical Technology and Applied Science (ICTAS).

DISCLOSURES

No conflicts of interest, financial or otherwise, are declared by the authors.

AUTHOR CONTRIBUTIONS

Author contributions: J.S.W., M.W.W., and J.J.S. conception and design of research; J.S.W., W.-K.L., and J.J.S. performed experiments; J.S.W. and J.J.S. analyzed data; J.S.W., W.-K.L., M.W.W., and J.J.S. interpreted results of experiments; J.S.W. prepared figures; J.S.W. and J.J.S. drafted manuscript; J.S.W., W.-K.L., M.W.W., and J.J.S. edited and revised manuscript; J.S.W., W.-K.L., M.W.W., and J.J.S. approved final version of manuscript.

REFERENCES

1. **Bartholomew GA, Lighton JRB.** Ventilation and oxygen consumption during rest and locomotion in a tropical cockroach, *Blaberus giganteus*. *J Exp Biol* 118: 449, 1985.
2. **Bradley TJ.** Control of the respiratory pattern in insects. *Hypoxia Circ* 618: 211–220, 2007.
3. **Buck J.** Some physical aspects of insect respiration. *Annu Rev Entomol* 7: 27–56, 1962.
4. **Chown S, Nicolson SW.** *Insect Physiological Ecology: Mechanisms and Patterns*. New York: Oxford University Press, 2004.
5. **Chown SL, Gibbs AG, Hetz SK, Klok CJ, Lighton JRB, Marais E.** Discontinuous gas exchange in insects: a clarification of hypotheses and approaches. *Physiol Biochem Zool* 79: 333–343, 2006.
6. **Chown SL, Marais E, Terblanche JS, Klok CJ, Lighton JRB, Blackburn TM.** Scaling of insect metabolic rate is inconsistent with the nutrient supply network model. *Funct Ecol* 21: 282–290, 2007.
7. **Corbet SA.** Pressure cycles and the water economy of insects. *Philos Trans R Soc London B, Biol Sci* 318: 377–407, 1988.
8. **Duncan FD, Förster TD, Hetz SK.** Pump out the volume—the effect of tracheal and subelytral pressure pulses on convective gas exchange in a

dung beetle, *Circellium bacchus* (Fabricus). *J Insect Physiol* 56: 551–558, 2010.
9. **Förster TD, Hetz SK.** Spiracle activity in moth pupae—the role of oxygen and carbon dioxide revisited. *J Insect Physiol* 56: 492–501, 2010.
10. **Gray IE.** Observations on the life history of the horned passalus. *Am Midl Nat* 35: 728–746, 1946.
11. **Greenlee K, Harrison J.** Development of respiratory function in the American locust *Schistocerca americana* I. Across-instar effects. *J Exp Biol* 207: 497, 2004.
12. **Greenlee K, Harrison J.** Development of respiratory function in the American locust *Schistocerca americana*: II. Within-instar effects. *J Exp Biol* 207: 509, 2004.
13. **Greenlee K, Harrison J.** Respiratory changes throughout ontogeny in the tobacco hornworm caterpillar, *Manduca sexta*. *J Exp Biol* 208: 1385, 2005.
14. **Greenlee KJ, Henry JR, Kirkton SD, Westneat MW, Fezzaa K, Lee WK, Harrison JF.** Synchrotron imaging of the grasshopper tracheal system: morphological and physiological components of tracheal hypermetry. *Am J Physiol Regul Integr Comp Physiol* 297: R1343–R1350, 2009.
15. **Greenlee KJ, Socha JJ, Eubanks HB, Thapa G, Pedersen P, Lee W-K, Kirkton SD.** Hypoxia-induced compression in the tracheal system of the tobacco hornworm caterpillar, *Manduca sexta* L. *J Exp Biol* In press.
16. **Harrison JF, Camazine S, Marden JH, Kirkton SD, Rozo A, Yang X.** Mite not make it home: tracheal mites reduce the safety margin for oxygen delivery of flying honeybees. *J Exp Biol* 204: 805–814, 2001.
17. **Harrison JF, Frazier MR, Henry JR, Kaiser A, Klok CJ, Rascon B.** Responses of terrestrial insects to hypoxia or hyperoxia. *Respir Physiol Neurobiol* 154: 4–17, 2006.
18. **Harrison JF, Waters JS, Cease AJ, Vandenbrooks JM, Callier V, Klok CJ, Shaffer K, Socha JJ.** How locusts breathe. *Physiology* 28: 18–27, 2013.
19. **Kaiser A, Klok CJ, Socha JJ, Lee WK, Quinlan MC, Harrison JF.** Increase in tracheal investment with beetle size supports hypothesis of oxygen limitation on insect gigantism. *Proc Natl Acad Sci USA* 104: 13198–13203, 2007.
20. **Klok CJ, Harrison JF.** Atmospheric hypoxia limits selection for large body size in insects. *PLos One* 4: e3876, 2009.
21. **Lehmann FO, Schützner P.** The respiratory basis of locomotion in *Drosophila*. *J Insect Physiol* 56: 543–550, 2010.
22. **Levy RI, Schneiderman HA.** Discontinuous respiration in insects-III. The effect of temperature and ambient oxygen tension on the gaseous composition of the tracheal system of silkworm pupae. *J Insect Physiol* 12: 105–121, 1966.
23. **Levy RI, Schneiderman HA.** Discontinuous respiration in insects. II. The direct measurement and significance of changes in tracheal gas composition during the respiratory cycle of silkworm pupae. *J Insect Physiol* 12: 83–104, 1966.
24. **Lighton JRB.** Discontinuous gas exchange in insects. *Annu Rev Entomol* 41: 309–324, 1996.
25. **Lighton JRB.** *Measuring Metabolic Rates: A Manual For Scientists*. New York: Oxford University, 2008, p. 201.
26. **Lighton JRB, Fukushi T, Wehner R.** Ventilation in *Cataglyphis bicolor*: regulation of carbon dioxide release from the thoracic and abdominal spiracles. *J Insect Physiol* 39: 687–699, 1993.
27. **Lighton JRB, Garrigan D.** Ant breathing: testing regulation and mechanism hypotheses with hypoxia. *J Exp Biol* 198: 1613–1620, 1995.
28. **Lighton JRB, Lovegrove BG.** A temperature-induced switch from diffusive to conective ventilation in the honeybee. *J Exp Biol* 154: 509–516, 1990.
29. **Marais E, Klok CJ, Terblanche JS, Chown SL.** Insect gas exchange patterns: a phylogenetic perspective. *J Exp Biol* 208: 4495–4507, 2005.
30. **Miller PL.** Ventilation in active and in inactive insects. In: *Locomotion and Energetics in Arthropods*, edited by Herreid CF and Fourtner CF. New York: Plenum, 1981, p. 367–390.
31. **R Development Core Team.** *R: A Language and Environment for Statistical Computing*. R Foundation for Statistical Computing, Vienna, Austria. http://www.R-project.org, 2011.
32. **Robertson CH Jr.** The anatomy of the respiratory system of the Passalus Beetle, *Popilius disjunctus* (Illiger). *Am Midl Nat* 68: 376–393, 1962.
33. **Schultz TD, Quinlan MC, Hadley NF.** Preferred body temperature, metabolic physiology, and water balance of adult *Cicindela longilabris*: a comparison of populations from boreal habitats and climatic refugia. *Physiol Zool* 65: 226–242, 1992.
34. **Socha JJ, Förster TD, Greenlee KJ.** Issues of convection in insect respiration: Insights from synchrotron X-ray imaging and beyond. *Respir Physiol Neurobiol* 173: S65–S73, 2010.
35. **Socha JJ, Lee WK, Harrison JF, Waters JS, Fezzaa K, Westneat MW.** Correlated patterns of tracheal compression and convective gas exchange in a carabid beetle. *J Exp Biol* 211: 3409–3420, 2008.
36. **Socha JJ, Westneat MW, Harrison JF, Waters JS, Lee WK.** Real-time phase-contrast x-ray imaging: a new technique for the study of animal form and function. *BMC Biol* 5: 6, 2007.
37. **Vogel S.** Living in a physical world. *J Biosci* 29: 391–397, 2004.
38. **Walker JA.** QuickImage: a modification of NIH Image with enhanced digitizing tools. http://www.usm.maine.edu/~walker/software.html.
39. **Webster MR, Vita RD, Twigg JN, Socha JJ.** Mechanical properties of tracheal tubes in the American cockroach (*Periplaneta americana*). *Smart Mater Struct* 20: 094017, 2011.
40. **Weis-Fogh T.** Functional design of the tracheal system of flying insects as compared with the avian lung. *J Exp Biol* 41: 207–227, 1964.
41. **Westneat MW, Betz O, Blob RW, Fezzaa K, Cooper WJ, Lee WK.** Tracheal respiration in insects visualized with synchrotron X-ray imaging. *Science* 299: 558–560, 2003.
42. **Westneat MW, Socha JJ, Lee WK.** Advances in biological structure, function, and physiology using synchrotron X-ray imaging. *Annu Rev Physiol* 70: 119–142, 2008.